Plastic ice in confined geometry: the evidence from neutron diffraction and NMR relaxation



2007 J. Phys.: Condens. Matter 19 415117

(http://iopscience.iop.org/0953-8984/19/41/415117)

IOP PUBLISHING JOURNAL OF PHYSICS: CONDENSED MATTER

J. Phys.: Condens. Matter **19** (2007) 415117 (12pp) doi:10.1088/0953-8984/19/41/415117

# Plastic ice in confined geometry: the evidence from neutron diffraction and NMR relaxation

**J Beau W Webber[1,2,3], John C Dore[2], John H Strange[2], Ross Anderson[1] and Bahman Tohidi[1]**

[1] Institute of Petroleum Engineering, Heriot Watt, Edinburgh EH14 4AS, UK
[2] School of Physical Sciences, University of Kent, CT2 7NH, UK
[3] Lab-Tools Ltd, G17, Canterbury Enterprise Hub, University of Kent, CT2 7NJ, UK

E-mail: J.B.W.Webber@kent.ac.uk

Received 7 May 2007, in final form 6 June 2007
Published 27 September 2007
Online at stacks.iop.org/JPhysCM/19/415117

**Abstract**

Neutron diffraction and nuclear magnetic resonance (NMR) relaxation studies have been made of water/ice in mesoporous SBA-15 silica with ordered structures of cylindrical mesopores with a pore diameter ∼8.6 nm, over the temperature range 180–300 K. Both measurements show similar depressed freezing and melting points due to the Gibb–Thomson effect.

The neutron diffraction measurements for fully filled pores show, in addition to cubic and hexagonal crystalline ice, the presence of a disordered water/ice component extending a further 50–80 K, down to around or below 200 K. NMR relaxation measurements over the same temperature range show a free induction decay that is partly Gaussian and characteristic of brittle ice but that also exhibits a longer exponential relaxation component. An argument has been made (Liu *et al* 2006 *J. Phys:. Condens. Matter* **18** 10009–28; Webber *et al* 2007 *Magn. Reson. Imag.* **25** 533–6) to suggest that this is an observation of ice in a plastic or rotationally mobile state, and that there is a fully reversible inter-conversion between brittle and plastic states of ice as the temperature is lowered or raised. More recent detailed NMR measurements are also discussed that allow the extraction of activation enthalpies and an estimate to be made of the equilibrium thickness, as a function of temperature, if the the assumption is made that the plastic component is in the form of a layer at the silica interface. The two different techniques suggest a maximum layer thickness of about 1.0–1.5 nm.

(Some figures in this article are in colour only in the electronic version)

  

## 1. Introduction

This paper reports a study of the behaviour of water and ice in a sample of templated SBA-15 porous silica with a pore diameter of ∼86 Å, over a wide temperature range, using both neutron diffraction measurements and NMR relaxation measurements.

The data presented here form part of a comprehensive investigation of water/ice in SBA-15 silicas using neutron diffraction and NMR techniques. The present case is for an 'over-filled' sample, and additional measurements for several 'partially filled' states using the same sample material will be presented in subsequent papers.

It is well known that the equilibrium melting phase transition is depressed by nano-structuring a sample, this behaviour being well described by the Gibbs–Thomson equation (Jackson and McKenna 1990), in the same way that nano-structuring changes the equilibrium vapour pressure, as described by the Kelvin equation (Thomson 1871). The technique of NMR cryoporometry (Strange *et al* 1993) makes use of the Gibbs–Thomson equation, and has proved to be highly useful in characterizing porous systems.

These techniques have been further developed, and also applied to a neutron diffraction (ND) methodology, whereby a set of measurements of the scattering from water/ice in a porous system is analysed to obtain the amplitudes of each scattering component, as a function of temperature. It is thus possible to obtain a neutron diffraction cryoporometry graph, from a detailed but otherwise standard neutron diffraction run, in the form of a set of melting/freezing graphs for each phase component in the system (Webber and Dore 2007). This data may then be interpreted by application of the Gibbs–Thomson equation, as per a standard NMR cryoporometry analysis, to identify which components of the water/ice system are in the pore and which are bulk components.

The graphs for each phase component show transitions between crystalline ice and water with melting point depressions similar to those observed by proton NMR cryoporometry, but in addition are able to discriminate between the transitions, and hence location, of cubic and hexagonal ice. They also show the presence of a disordered phase, water-like as far as the neutron diffraction measurements were able to resolve, but extending below the conventional Gibbs–Thomson depressed melting/freezing points, down to below −50 °C, with a significant amplitude at −80 °C.

To probe the nature of this disordered component further, the dynamics of this system were studied by NMR proton relaxation: the value of the NMR transverse ($T_2$) spin–spin relaxation rate gives information about the dynamics of the protons in the confined material as a function of temperature (Torrey 1953, Chezeau and Strange 1979, Booth and Strange 1998). There is usually a large difference in the $T_2$ values between the liquid and solid phases, and this serves to distinguish between these states in the cryoporometry studies. However, the actual relaxation rates themselves give additional information about the proton mobility.

In this case, the NMR relaxation rates for this disordered component suggest that, rather than being in a liquid state, as discussed in earlier publications (Topgaard and Soderman 2002, Crupi *et al* 2003), this component over most of this temperature range has minimal translational motion, and thus must be in an ice-like form. The detailed NMR behaviour shown by this component is indicative of the presence of rotational motion, suggesting that this ice has characteristics similar to a plastic crystal.

## 2. Preparation and characterisation of an SBA-15 sample

A templated mesoporous silica sample with ordered cylindrical pores was used to nano-structure the water/ice system. The SBA-15 silica was synthesized by the method reported

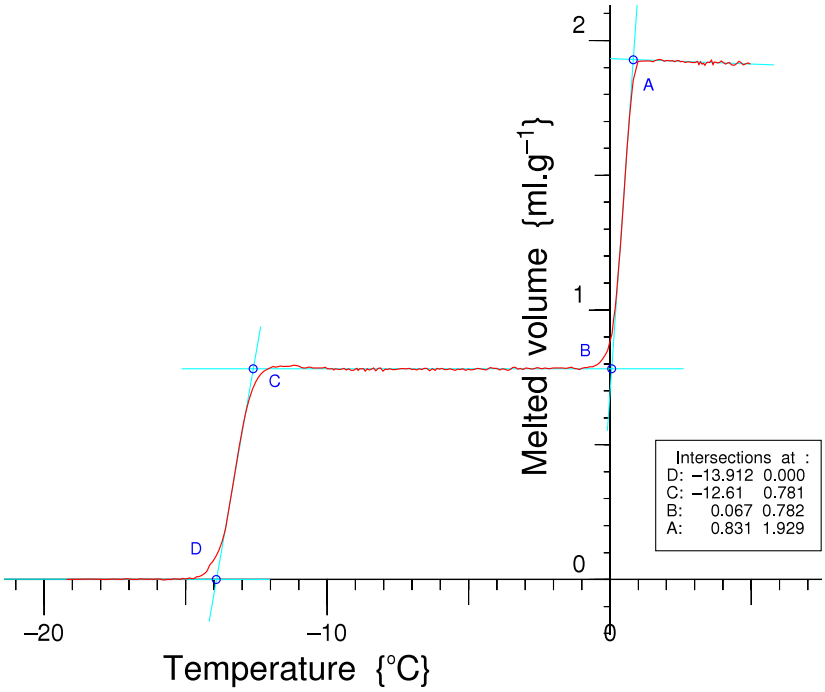


**Figure 1.** NMR cryoporometric melting curve for $H_2O$ in SBA-15 TLX-1-5 (F5) templated silica, at a warming rate of 0.05 °C min$^{-1}$.

by Zhao *et al* (1998a), (1998b). Details of the thermal treatment and calcination of the sample are given elsewhere (Schreiber *et al* 2001). The pore structure of the calcined SBA-15 silica was characterized by nitrogen adsorption, x-ray diffraction (XRD), differential scanning calorimetry (DSC) thermoporosimetry and NMR cryoporometry (Liu *et al* 2006).

## 3. NMR cryoporometry

A highly informative technique for studying phase changes in a confined geometry is NMR cryoporometry (Strange *et al* 1993, Webber 2000, Webber *et al* 2001), which uses a measurement of the NMR signal amplitude to study the water/ice system in the pores. The magnitude of the transverse relaxation signal ($T_2$), at a time when the signal from the solid has decayed, is used to indicate the quantity of liquid in the sample material at a particular temperature. The Gibbs–Thomson equation may then be applied to this information, both to determine which fractions of the crystalline/liquid system are in the pores and to obtain a pore-size distribution function. NMR cryoporometry is a development of DSC thermoporosimetry, but offers a number of advantages, as has been discussed earlier (Dore *et al* 2004, Webber and Dore 2004).

The melting point of the pore liquid is depressed by $\Delta T_m$, as given by the Gibbs–Thomson relation (Jackson and McKenna 1990)

$$\Delta T_m = T_m^{\infty} - T_m(x) = \frac{4\sigma_{cl} T_m}{x \Delta H_f \rho_s} \cos(\phi) \tag{1}$$

where $T_m^{\infty}$ is the bulk melting point of the solid (considered to be a crystal of infinite size), $T_m(x)$ is the melting point of crystals of diameter $x$, $\sigma_{sl}$ is the surface energy at the crystal–

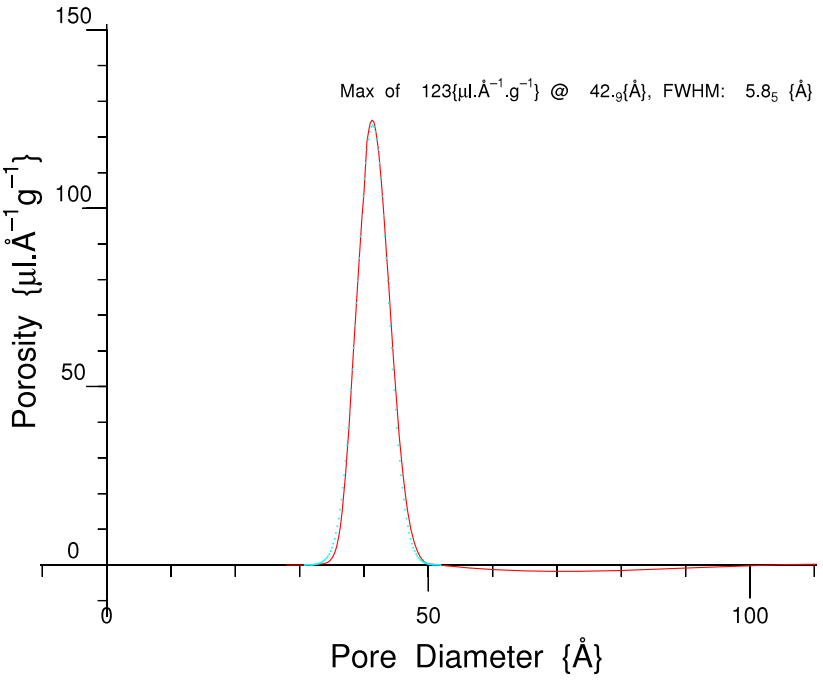


**Figure 2.** Pore size distribution, for $H_2O$ in SBA-15 (F5) templated silica, from NMR cryoporometry.

liquid interface, $\Delta H_f$ is the bulk enthalpy of fusion (per gram of material), $\rho_s$ is the density of the solid, and $\phi$ is the contact angle of the solid–liquid interface at the pore wall.

This may be written more simply in the form (Strange *et al* 1993):

$$\Delta T_m = \frac{K_{GT}}{x} \tag{2}$$

where $x$ is a dimension that defines the effective size of the pore and $K_{GT}$ is a constant that depends on the liquid, the pore geometry and the wetting nature of the pore walls.

More specifically,

$$\Delta T_m = \frac{k_{GT}}{x} = \frac{k_g k_l k_i}{x}. \tag{3}$$

If, with suffixes l for liquid, s for solid, and p for pore wall, we apply the Young equation $\sigma_{pl} = \sigma_{sl}\cos(\phi) + \sigma_{ps}$ and the Young–Dupré equation $W_{ps} = \sigma_{sl} + \sigma_{pl} - \sigma_{ps} =$ the reversible work required to separate unit area of the solid from the pore wall (Defay *et al* 1951, Gregg and Sing 1967), then we obtain

$$\cos(\phi) = \left(\frac{W_{ps}}{\sigma_{sl}} - 1\right). \tag{4}$$

Then $k_g$ is a geometric constant that is dependent on the interfacial shape (Webber 2003), $k_l = \frac{T_m^\infty}{\Delta H_f \rho_s}$ is a constant specific to the crystal thermodynamic parameters, and $k_i = \sigma_{sl} - W_{ps}$ is a constant specific to the two inter-surface interaction terms of the crystal.

The freezing phase transition is normally a non-equilibrium process controlled by supercooling, and thus the equilibrium melting transition has commonly been used to study these systems. Figure 1 shows the quantity of water that has melted in these pores as a function of

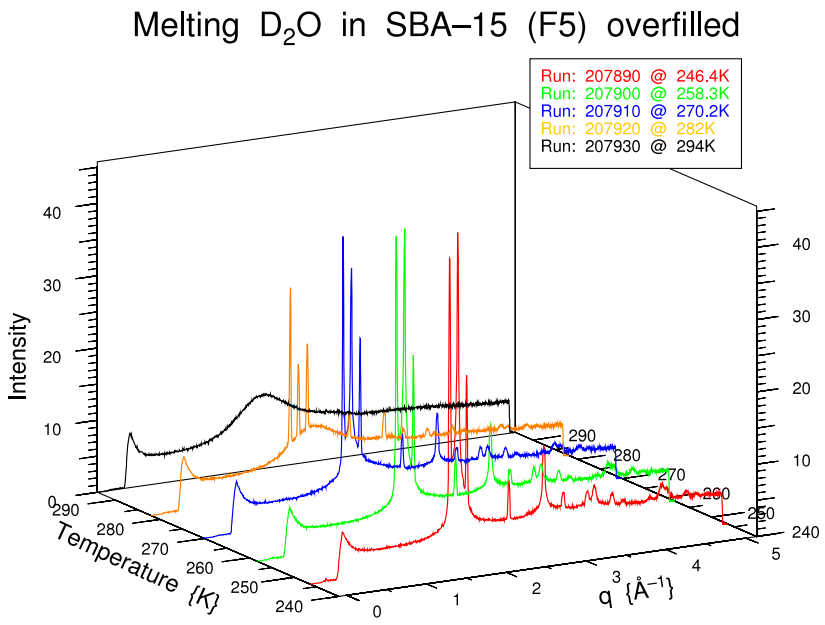


**Figure 3.** Neutron diffraction curves for the melting of ice to water in overfilled SBA-15 (F5) silica.

temperature, and the sharpness of the melting event at −13 °C demonstrates well the monomodal nature of the porosity in SBA-15 silicas. The additional melting event corresponds to the melting of bulk ice around the grains, these two plateaux allowing the pore volume of the pores to be determined. By applying the Gibbs–Thomson relationship to this data, a pore size distribution may also be obtained (Strange *et al* 1993), as shown in figure 2.

Recently a technique to also observe an equilibrium freezing transition has been reported independently by Petrov and Furo (2006) and Webber *et al* (2007).

## 4. Neutron diffraction cryoporometry

For the neutron experiments, a fixed quantity of $D_2O$ water was added to the dry silica powder and the sample left to equilibriate. This produced an 'over-filled' sample with a filling factor, $f$, slightly larger than unity.

Measurements were made using the D20 diffractometer (Hansen 2004) at the Institut Laue-Langevin (ILL) in Grenoble, France. The high neutron flux on this instrument meant that a measurement of only 2 min was sufficient to give a diffraction pattern with good statistics, as shown in figure 3. Diffraction measurements were made using a scanning temperature ramp of 0.6 K $min^{-1}$, first cooling and then warming. A preliminary report of this work has been given by Liu (Liu 2003), with a more detailed analysis given later (Liu *et al* 2006).

Figure 3 shows a selection of datasets, measured on the warming run, plotting every tenth diffraction curve. At the highest temperatures there is a broad liquid–water peak; at lower temperatures the signal shows the hexagonal ice melting to water, and at yet lower temperatures there is a complex inter-conversion between defective cubic ice, hexagonal ice and a water-like component.

Figure 5 was obtained using an algorithm that uses a linear least-squares algorithm to optimize linear combinations of the three template curves for the three phases (figure 4). This

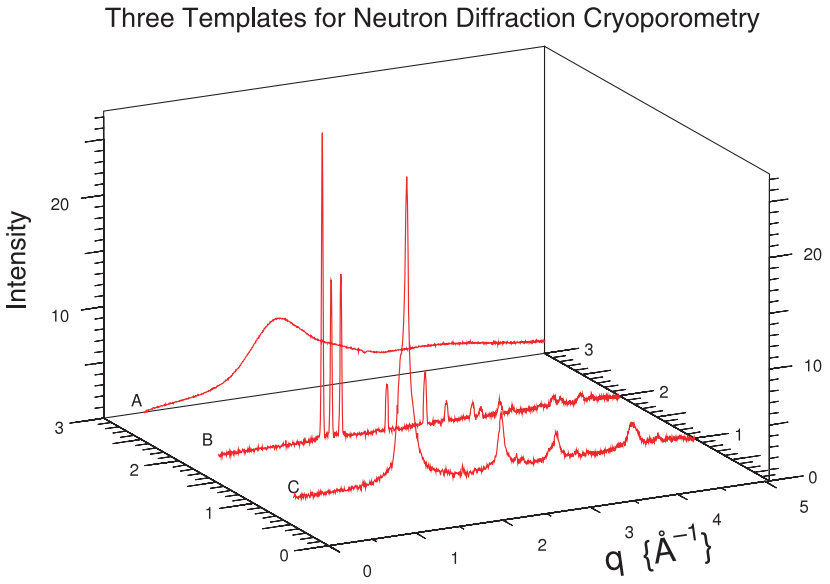


**Figure 4.** Neutron diffraction curves for three ice/water phases: (A) water, (B) hexagonal ice, (C) defective cubic ice.

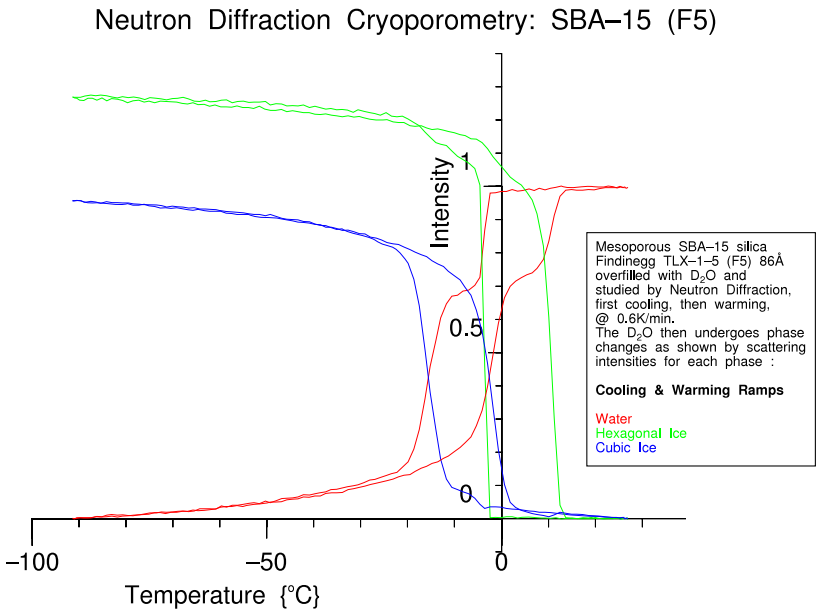


**Figure 5.** Neutron diffraction cryoporometric curves for ice/water freezing and melting in overfilled SBA-15 (F5) templated silica with a nominal pore diameter of 86 Å, showing the separately resolved data for cubic ice, hexagonal ice and water.

acts so as to morph, at each measured temperature, a combined curve that forms the best match to the measured data. The resultant ND cryoporometric curves are obtained for not only the water phase but also for the brittle hexagonal and cubic ice components, which is something that

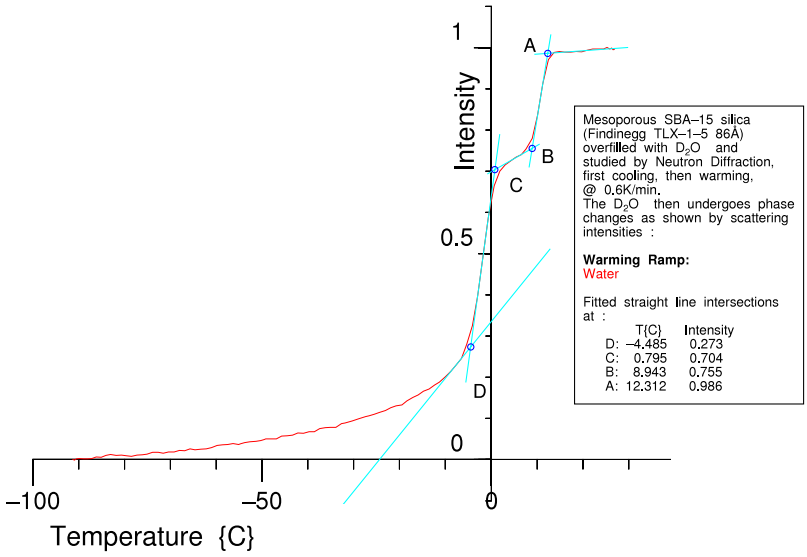


**Figure 6.** Neutron diffraction cryoporometry curves for water melting in overfilled SBA-15 (F5) templated silica with a nominal pore diameter of 86 Å, showing disordered component between −80 and −5 °C.

NMR cryoporometry cannot do. They show good agreement with results from a conventional peak amplitude analysis (Liu *et al* 2006, figure 9).

The hexagonal ice can be seen to melt mainly at temperatures appropriate to bulk $D_2O$ ice (allowing for instrumental effects), while the cubic ice forms at a lowered temperature appropriate to the Gibbs–Thomson melting point reduction in these pores, indicating that it is forming in the pores, in accordance with previous studies on sol–gel silicas with pores of <30 nm diameter. However, a further 10% of the hexagonal ice is also seen to form at a reduced temperature, indicating that some of the ice in the pores of the SBA-15 incorporates a hexagonal component.

As the temperature is further lowered, the quantity of the disordered component decreases, converting primarily to further cubic ice, but some clearly also converts to hexagonal ice. As the temperature is again increased, the crystalline ices reversibly transform back to the disordered component, indicating a surprising equilibrium between the separate phases.

The extraction of robust parameters for the water melting curve (figure 6) clearly shows the disordered component that is best matched by the water template. However, a study of the actual diffraction data shows a difference from the bulk water curves. This component exists below the normal Gibbs–Thomson depressed temperature for $D_2O$ water in these pores, extending a further 50–80 K, down to around or below 200 K, and may be indicative of the presence of some form of amorphous ice.

The quantity of the disordered ice may be determined from the linearized fits to the water dataset, and these indicate that the maximum quantity of the plastic ice amounts to about 0.4 of the total $D_2O$ in the pore. If it is assumed that the plastic ice forms near the pore surface, this value suggests that the maximum layer thickness is around 0.94 nm, for 8.6 nm diameter cylindrical pores.

There is a clear interest in studying the dynamics of this disordered component, particularly with regard to quantifying the translational and rotational components. Information on the dynamical state of the confined water/ice can be obtained by NMR measurement of the

transverse spin–spin $T_2$ relaxation time for $H_2O$ water as a function of temperature. Such measurements were the next to be performed, following the measurement of these neutron diffraction cryoporometry results.

## 5. NMR relaxation studies

A similarly slightly overfilled sample of the templated SBA silica ($f = 1.2$) using $H_2O$ water was studied as a function of temperature by proton nuclear magnetic resonance (NMR) relaxation. Earlier papers give some of the details (Dore *et al* 2004, Webber and Dore 2004, Liu *et al* 2006) but the essential information relevant to the current discussion is briefly presented, prior to discussing more recent conclusions. The variation of the NMR $T_2$ relaxation rate with temperature was measured on the same apparatus as was previously used for NMR cryoporometry studies (Webber *et al* 2001, Webber and Dore 2004).

Over the lower-to-middle temperature range, the relaxation rate was measured by recording the Bloch decay from the water/ice. The dataset was fitted using the sum of a Gaussian function appropriate to the brittle ice and an exponential function appropriate to the more mobile component. The measured amplitudes were then corrected for the natural $T_2^*$ due to the gradients in the $B_0$ magnetic field. At medium-to-higher temperatures, a chain of echoes was also recorded using a Carr–Purcell–Meiboom–Gill (CPMG) sequence.

The NMR relaxation behaviour observed for the water/ice in SBA-15 porous silica is dependent on temperature and, as well as 'water-like' and 'ice-like' phases, a phase with intermediate properties is observed. Pure bulk water has a $T_2$ relaxation time of the order of a few seconds at the 0.5 T $B_0$ static magnetic field used for this relaxation work. However, in the pores of this SBA-15 silica, the surface relaxivity reduces the $T_2$ of the water to about 8 ms. In comparison, the bulk phase of brittle ice has an approximately Gaussian free induction decay with a relaxation time of the order of 10 $\mu$s.

The free induction decay (FID) for this sample at ∼190 K is very similar to that of bulk ice but, as the temperature is raised by 20–210 K, some of the brittle ice transforms to a component with a longer relaxation time and with a form that becomes increasingly exponential. Measurement of the variation of the $T_2$ relaxation rate with temperature for this longer relaxation component, as measured by Carr–Purcell–Meiboom–Gill (CPMG) and $T_2^*$ corrected FID, is given in figure 7.

Above 180 K, the shorter brittle ice component reduces in amplitude as it converts to the longer form, while the longer component of the FID remains fairly constant in relaxation time, between 100 and 200 $\mu$s, and its amplitude progressively increases with temperature (figure 8). Just below the melting temperature of the ice in the pores, at the Gibb–Thomson lowered temperature of about 260 K, there is a rapid increase in the relaxation time of the longer component. Neutron diffraction measurements show a similar component, as a broad peak characteristic of defective ice/water.

There are three possible causes that need to be considered for this factor of ten increase in the $T_2$ at around 200–220 K, for the defective ice, over that for brittle ice; these are discussed in detail elsewhere (Liu *et al* 2006):

(i) $T_2$ relaxation is due to the dipolar interaction of one nuclear spin on another; an increase in the actual distance between the protons will lengthen $T_2$. Given the observed changes as a function of temperature in figure 8, it is improbable that this behaviour is due to a simple lattice expansion.

(ii) There may be translational diffusion, giving rise to motional narrowing. This may be expected to play a part in the observed $T_2$, particularly given the large change in

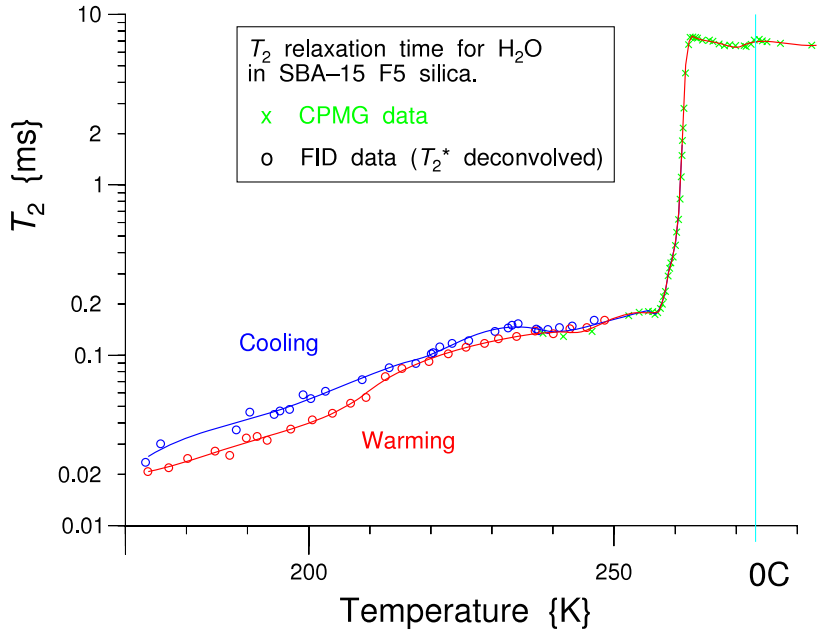


**Figure 7.** Variation with temperature of the NMR long $T_2$ relaxation time component for plastic ice in SBA-15 porous silica.

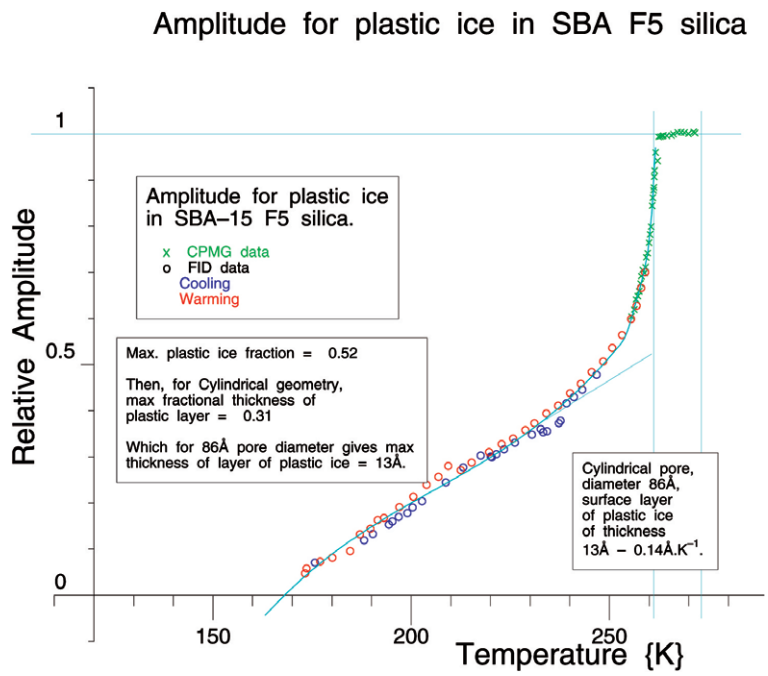


**Figure 8.** Amplitude of NMR signal for plastic ice in SBA-15.

temperature, and is the likely cause of the rapid change in $T_2$ in the vicinity of the melting point in the pores. However, the observed behaviour of $T_2(T)$ over the range 180–250 K is not characteristic of a translational activation energy, as would be expected for translational motional narrowing.

(iii) There may be rotational diffusion. In plastic crystals, rotation is well known to give rise to a form of motional averaging such that the actual proton separations must be replaced by the separation of the molecular centres. This gives rise to a significant increase in $T_2$ at the onset of rotational motion, followed by a plateau in $T_2(T)$ as $T$ increases (Chezeau and Strange 1979).

The plot of $T_2(T)$ in figure 7 is very similar to that for the plastic phases of materials such as cyclohexane, showing the form of the above case (iii) with a step and plateau, followed by the rapid rise of case (ii) just before melting; consequently it is suggested that this longer ice component is in a plastic crystalline state and that this plastic ice corresponds to the disordered component, as measured by neutron scattering.

Thus the rise in the 180–230 K region is due to the onset of rotational motion, which is well known to give rise to a form of motional averaging such that the actual proton separations must be replaced by the separation of the molecular centres. This gives rise to a significant increase in $T_2$ at the onset of rotational motion, followed by a plateau in $T_2(T)$ as $T$ increases (Chezeau and Strange 1979). Translational motion sets in just prior to the melting event.

Consequently, it is suggested that this longer ice component is in a plastic crystalline state and that this plastic ice corresponds to the disordered component, as measured by neutron scattering. These NMR measurements indicate that there is an equilibrium state within the interfacial layer in the pores, such that the ice changes continuously and reversibly with temperature between a brittle cubic crystalline phase and a plastic disordered rotator phase.

Figure 8 shows data for the fractional amplitude of this longer relaxation component, with corrections for receiver linearity and also changes with temperature of the Boltzmann population and NMR coil Q. These measurements indicate that the fraction of plastic ice in the pores increases from about 0.05 at 170 K to an extrapolated maximum of about 0.52 of the total volume at the melting point in the pores at about 260 K. As this melting point is approached the amplitude data for the longer component also includes the amplitude of any fraction with increased translational motion, and so increases rapidly. If one assumes that the plastic ice is in the form of a layer on the surface of cylindrical pores, the maximum extrapolated fractional thickness is 0.31. For 8.6 nm diameter pores this corresponds to a maximum layer thickness of about 1.3 nm, decreasing at about 0.014 nm $K^{-1}$ as the temperature is lowered.

If the NMR $T_2$ relaxation data for this longer relaxation component is plotted against inverse temperature as an Arrhenius graph (figure 9), the activation enthalpy for the sloping part of a cooling ramp over the temperature range 180–230 K may be determined as 4.6 kJ $mol^{-1}$. This is believed to be due to the onset of rotational motion. The warming ramp profile is not identical to that of the cooling ramp, but at this stage it is not clear if this is an instrumental effect or not.

At higher temperatures there is the plateau that is believed to relate to the dynamical region where rotational motion is probably still increasing, but where, for the purposes of NMR relaxation (as discussed earlier), the effective proton separations just average to a constant value equal to the molecular-centre separations. If this plateau is fitted with a constant amplitude, and this is then subtracted from the $T_2$ relaxation data on the Arrhenius graph, a further straight line is obtained. Currently, it is believed that this component represents the onset of translational motion, with a surprisingly large enthalpy of 810 kJ $mol^{-1}$.

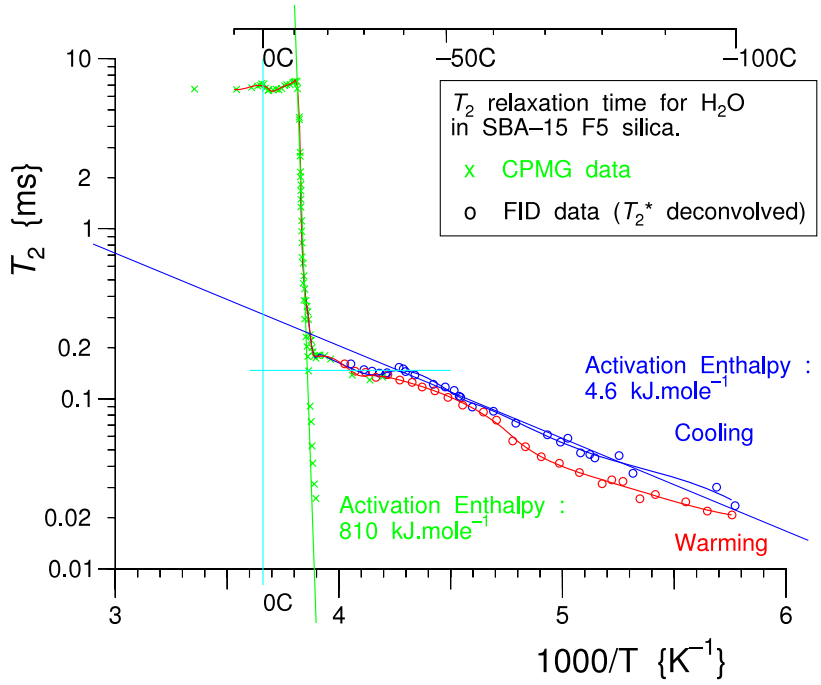


**Figure 9.** Variation with temperature of the long $T_2$ relaxation time component for plastic ice in SBA-15 porous silica-Arrhenius plot.

## 6. Conclusions and future experiments

The present study extends the general investigation of super-cooling and nucleation features for water in ordered mesoporous silicas, using neutron diffraction cryoporometry and NMR relaxation.

It is believed that these results indicate that the water/ice system in SBA-15 pores can form a disordered plastic ice phase, possibly as an amorphous ice in the form of a layer on the pore surface, whose quantity depends on temperature. If this quantity is interpreted as a layer, neutron scattering cryoporometry suggests a maximum layer thickness of around 1 nm in 8.6 nm pores, while the very different technique of NMR relaxation suggests a thickness of around 1.3 nm.

There is a clear interest in studying the dynamics of this plastic ice, particularly with regard to quantifying the translational and rotational components, and NMR spin–spin $T_2$ relaxation measurements have been shown to be highly informative. NMR spin–lattice $T_1$ relaxation measurements are currently under way and NMR rotating-frame $T_{1\rho}$ measurements are planned. Preliminary NMR field-cycling measurements have also been made to study the dynamics, and further measurements are planned. NMR magnetic gradient techniques, both pulsed-field-gradient (PFG) and fringe-field-gradient methods, are useful techniques to measure translational motion and can also be used to provide further information relating to self-diffusion in the pore network.

Quasi-elastic neutron scattering (QENS) is clearly a preferred technique for characterizing such systems, and such measurements have previously been made on water in porous Vicor glass (Zanotti *et al* 2005), which were described as indicating the presence of a liquid–liquid

transition. QENS measurements are now in preparation on water in mono-modal SBA-15 systems and may help to distinguish between translational motion and rotational motion.

## Acknowledgments

The neutron work at the Institut Laue-Langevin, France was undertaken within the UK Engineering and Physical Sciences Research Council (EPSRC) programme for access to neutron facilities. The work of Beau Webber was partially supported by collaborations with the BMFFFS Project (behaviour and modelling of faults/fractures/fluids systems) and the Centre for Gas Hydrate Research, both in the Institute of Petroleum Engineering, Heriot-Watt University, UK. The work in Berlin was supported by the Deutsche Forschungsgemeinschaft in the framework of the SFB 448 'Mesoscopically Organised Composites'. We are indebted to professor Gerhard Findenegg and Dr Sylvia Reinhard for the preparation of the SBA-15 sample. We thank Thomas Hansen for assistance with the neutron measurements on the D20 diffractometer at ILL.

## References

Booth H F and Strange J H 1998 *Magn. Reson. Imag.* **16** 501–4
Chezeau J M and Strange J H 1979 *Phys. Rep.* **53** 1–92
Crupi V, Majolino D, Migliardo P, Venuti V and Bellissent-Funel M C 2003 *Mol. Phys.* **101** 3323–33
Defay R, Prigogine I, Bellemans A and Everett D H 1951 *Surface Tension and Adsorption* (in French)
Defay R, Prigogine I, Bellemans A and Everett D H 1966 *Surface Tension and Adsorption* (London: Longmans, Green & Co) (Engl. Transl.)
Dore J C, Webber J B W and Strange J H 2004 *Colloids Surf.* A **241** 191–200
Gregg S J and Sing K S W 1967 *Adsorption, Surface Area and Porosity* 2nd edn (London: Academic)
Hansen T 2004 The D20 instrument description, http://whisky.ill.fr/YellowBook/D20/
Jackson C L and McKenna G B 1990 *J. Chem. Phys.* **93** 9002–11
Liu E 2003 Synthesis of ordered mesoporous aluminium oxide using novel templating techniques, and the characterisation of nucleation of ice in mesoporous silica *Msc Physics* University of Kent at Canterbury, UK
Liu E, Dore J C, Webber J B W, Khushalani D, Jähnert S, Findenegg G H and Hansen T 2006 *J. Phys.: Condens. Matter* **18** 10009–28 http://stacks.iop.org/0953-8984/18/10009
Petrov O and Furo I 2006 *Phys. Rev.* E **73** 7
Schreiber A, Ketelsen I and Findenegg G H 2001 *Phys. Chem. Chem. Phys.* **3** 1185–95
Strange J H, Rahman M and Smith E G 1993 *Phys. Rev. Lett.* **71** 3589–91
Thomson W 1871 *Phil. Mag.* **42** 448–52
Topgaard D and Soderman O 2002 *Biophys. J.* **83** 3596–606
Torrey H C 1953 *Phys. Rev.* **92** 962
Webber B and Dore J 2004 *J. Phys.: Condens. Matter* **16** S5449–70 (Special Issue: Water in Confined Geometry) http://stacks.iop.org/JphysCM/16/S5449
Webber J B W 2000 The characterisation of porous media *PhD Physics* University of Kent at Canterbury, UK http://www.kent.ac.uk/physical-sciences/publications/theses/jbww.html
Webber J B W 2003 *Magn. Reson. Imag.* **21** 428
Webber J B W, Anderson R, Strange J H and Tohidi B 2007 *Magn. Reson. Imag.* **25** 533–6
Webber J B W and Dore J C 2007 submitted
Webber J B W, Strange J H and Dore J C 2001 *Magn. Reson. Imag.* **19** 395–9
Zanotti J M, Bellissent-Funel M C and Chen S H 2005 *Europhys. Lett.* **71** 91–7
Zhao D Y, Feng J L, Huo Q S, Melosh N, Fredrickson G H, Chmelka B F and Stucky G D 1998a *Science* **279** 548–52
Zhao D Y, Huo Q S, Feng J L, Chmelka B F and Stucky G D 1998b *J. Am. Chem. Soc.* **120** 6024–36